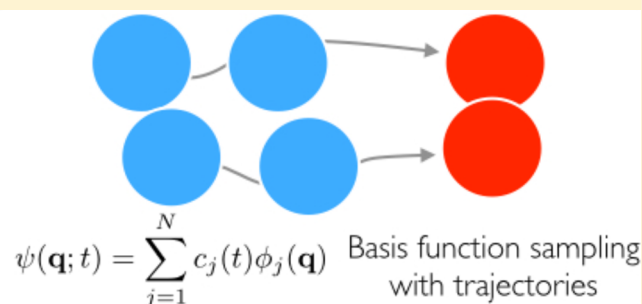


# Basis Set Generation for Quantum Dynamics Simulations Using Simple Trajectory-Based Methods

Maximilian A. C. Saller and Scott Habershon\*

Department of Chemistry and Centre for Scientific Computing, University of Warwick, Coventry, CV4 7AL, United Kingdom

**ABSTRACT:** Methods for solving the time-dependent Schrödinger equation generally employ either a global static basis set, which is fixed at the outset, or a dynamic basis set, which evolves according to classical-like or variational equations of motion; the former approach results in the well-known exponential scaling with system size, while the latter can suffer from challenging numerical problems, such as singular matrices, as well as violation of energy conservation. Here, we suggest a middle road: building a basis set using trajectories to place time-independent basis functions in the regions of phase space relevant to wave function propagation. This simple approach, which potentially circumvents many of the problems traditionally associated with global or dynamic basis sets, is successfully demonstrated for two challenging benchmark problems in quantum dynamics, namely, relaxation dynamics following photoexcitation in pyrazine, and the spin Boson model.



## 1. INTRODUCTION

Most methods for directly solving the time-dependent Schrödinger equation (TDSE)<sup>1</sup> introduce a linear combination of basis functions as a wave function *ansatz*,

$$|\psi(t)\rangle = \sum_{j=1}^n c_j(t) |\phi_j\rangle \quad (1)$$

where  $c_j(t)$  is a complex expansion coefficient and  $|\phi_j\rangle$  is the corresponding basis function (which may comprise both nuclear and electronic degrees-of-freedom). Quantum dynamics methods employing this *ansatz* can be further subdivided into (i) those methods employing a time-independent basis set that is chosen at the outset,<sup>1–4</sup> and (ii) those methods in which the basis functions are themselves time-dependent, for example, through the temporal behavior of a set of parameters.<sup>5–18</sup> In both cases, the time evolution of the linear expansion coefficients is derived by application of the Dirac–Frenkel variational principle;<sup>19–22</sup> however, while the same variational approach can (and has) been applied to derive equations of motion for the basis function parameters,<sup>23–25</sup> it is more common to adopt approximate methods such as classical molecular dynamics (MD) or Ehrenfest trajectories.

These two approaches have distinct advantages and disadvantages. Using a time-independent basis set reduces the problem to solution of a system of linear equations describing the evolution of the expansion coefficients, but choosing a small basis set that can accurately represent the wave function at all times and across all configurational space is a major difficulty; indeed, one is usually forced to choose a global basis set that spans the entire phase space of the problem, leading to redundancy and the well-known exponential-scaling problem associated with solution of the TDSE. This difficulty is avoided

in the case of time-dependent basis functions, where the underlying potential energy surface naturally guides basis set evolution toward relevant regions of configuration space. However, unless the basis set evolution is performed variationally, the time dependence of the basis set can violate the conservation of energy, which is implicit in the TDSE;<sup>17</sup> furthermore, even under variational evolution, numerical difficulties related to ill-conditioning of the evolution equations can arise, meaning that converging on the correct quantum-mechanical solution is itself a challenge.<sup>26</sup>

In this paper, we propose and test a “middle road” for quantum dynamics simulations: we use computationally inexpensive trajectory simulations to sample basis functions that are subsequently employed as a time-independent basis set for solution of the TDSE. The rationale for this approach is quite clear; for any given initial wave function, we assume that the region of phase space that will be sampled during wave function propagation can be accessed by a set of trajectories with appropriate initial conditions. By using trajectory-based simulations to place basis functions, the underlying assumption is that these trajectories will at least sample the correct regions of phase space; this is a much less stringent demand of the trajectory simulations than expecting them to accurately describe the evolving wave function across all configuration space at each given instance of time. In other words, our trajectories only have to visit those regions of configuration space that will be relevant to wave function propagation *at some point*; the exact time dependence of the wave function is addressed separately, using the complete set of basis functions sampled by the trajectories. We note that our approach is

Received: July 23, 2014

Published: November 25, 2014



distinct from other methods using adaptive basis sets (particularly, the basis expansion leaping (BEL)<sup>27</sup> and matching pursuit/split-operator Fourier transform<sup>28,29</sup> methodologies). In both cases, the movement of basis functions through phase space is generally driven by an optimization process in which one aims to keep the basis set that describes the propagating wave function as small as possible; in contrast, our methodology employs physically motivated trajectory simulations to restrict basis functions to the relevant region of phase space from the outset. As noted later, our approach does not employ coordinate grids at any level (as in the Matching Pursuit/Split Operator Fourier Transform [MP/SOFT] method) and is immediately employable to systems with at least 30 degrees of freedom, whereas BEL has been demonstrated for systems with just three degrees of freedom to date. In fact, our approach is somewhat similar in spirit to the Herman–Kluk semiclassical initial value representation (HK-SCIVR) method, which has found application in a wide variety of complex systems;<sup>30–33</sup> the most important differences are that the time-dependent expansion coefficients that define our wave function are fully coupled and obey a variational principle, in contrast to the assumptions that lead to the HK-SCIVR method.<sup>33</sup> As a final point of comparison, we note that the methodology proposed here is distinct from previous works that employed classical trajectories to generate an environment for the propagation of quantum degrees of freedom. For example, the classically-based separable potential (CSP) method propagates a Hartree-product-type wave function for a subset of quantum nuclei in an effective potential generated by the remaining classical nuclei;<sup>9</sup> related methods have similarly employed a trajectory-based treatment of classical nuclei, but with grid-based treatment of the quantum nuclei.<sup>34,35</sup> This idea of using classical trajectories to provide a time-dependent potential energy surface for quantum nuclei is certainly interesting, but is inherently distinct from the approach demonstrated here, wherein classical mechanics is used to generate a basis set prior to TDSE solution.

Our approach has several potential advantages. Unlike the global approach, the basis functions are only placed in regions of configuration space that are directly relevant to the problem at hand; this is a result of using trajectories that evolve under the influence of the potential energy surface. As a result, we reduce redundancy, circumvent the exponential size-scaling of the basis set, and replace it with a scaling that is dependent instead on the time scale of the problem and the number of trajectories that we are willing to perform. Furthermore, by adopting a time-independent (albeit trajectory-guided) basis set, we avoid both the computationally expensive propagation of the basis functions associated with variational evolution<sup>23–25</sup> and the problem of energy nonconservation associated with more approximate basis function evolution.<sup>17</sup> Finally, anticipating future applications to modeling electronically excited state dynamics in molecular systems, our approach is consistent with the local nature of *ab initio* electronic structure calculations; in other words, *ab initio* methods may be used during the trajectory simulations, and the resulting energies, forces and electronic wave functions can later be used in assessing Hamiltonian matrix elements for solution of the TDSE. Of course, we pay a price for these advantages; in particular, it is not clear *a priori* which trajectories we should use and how many basis functions we should sample in a given problem.

## 2. THEORY

Putting these problems aside for now, let us outline the method adopted here. To demonstrate our approach, we will consider a system comprising a set of nuclear degrees of freedoms, labeled  $\mathbf{q}$ , and a set of diabatic electronic states  $|\alpha\rangle$ . We assume that we have an initial wave function at  $t = 0$ ,  $|\psi(\mathbf{q};0)\rangle|\alpha\rangle$ , and our aim is to determine the wave function at a later time  $t$  by solution of the TDSE.

We first initiate a set of  $m$  trajectories, with initial conditions chosen to be representative of  $\psi(\mathbf{q};0)$ ; an obvious approach might be to sample initial positions and momenta from the corresponding Wigner distribution. These trajectories, which might be classical MD trajectories, Ehrenfest trajectories, or some other approximate method, are then propagated for a total of  $n_t$  time steps during which the coordinates and momenta of each trajectory are periodically stored with a probability of  $1/n_s$ . Here,  $n_s$  is a user-defined factor which, along with  $m$ , controls the total size of the basis set.

The basis set used in subsequent solution of the TDSE then comprises the complete set of  $N \approx m \times (n_t/n_s)$   $f$ -dimensional Gaussian wavepackets (GWPs) of the form

$$\langle \mathbf{q} | g_j \rangle = N_j \exp \left[ -(\mathbf{q} - \mathbf{q}_j)^T \mathbf{A}_j (\mathbf{q} - \mathbf{q}_j) + \left( \frac{i}{\hbar} \right) \mathbf{p}_j \cdot (\mathbf{q} - \mathbf{q}_j) \right] \quad (2)$$

where  $N_j$  is the appropriate GWP normalization constant,  $\mathbf{A}_j$  is an  $f \times f$  diagonal matrix with entries  $\gamma_\kappa/\hbar$ , where  $\kappa$  labels the degree of freedom, and  $\{\mathbf{q}_j, \mathbf{p}_j\}$  are the position and momenta of the corresponding trajectory. In other words, we use trajectories to generate a large set of GWP basis functions on a nonuniform grid; because these basis functions are sampled from trajectories originating from the phase space spanned by  $\psi(\mathbf{q};0)$ , our assumption is that they are most relevant for propagation of  $\psi(\mathbf{q};0)$ . Finally, we note that all calculations here use fixed-width GWPs; in other words,  $\gamma_\kappa$  is a constant for each degree of freedom  $\kappa$ .

After generating the GWP basis set, we solve the TDSE to give the time evolution of the linear expansion coefficients in eq 1. Assuming that we have available a set of diabatic electronic states (as in the problems to be treated below), our *ansatz* for the total wave function of the system is

$$\psi(\mathbf{q}; t) = \sum_{j=1}^n c_j(t) |g_j\rangle |\alpha_j\rangle \quad (3)$$

where  $|\alpha_j\rangle$  labels the diabatic state for basis function  $j$ . Applying the time-dependent variational principle,<sup>19–22</sup> the time dependence of the coefficients is given by

$$\dot{\mathbf{c}} = -\left( \frac{i}{\hbar} \right) \mathbf{S}^{-1} \mathbf{H} \mathbf{c} \quad (4)$$

where  $\mathbf{S}$  and  $\mathbf{H}$  are, respectively, the overlap and Hamiltonian matrices evaluated in the GWP basis set. The trajectory-guided approach taken in this work is schematically compared to more standard methods for solving the TDSE in Figure 1.

The final aspect of our basis set sampling strategy relates to the positioning of GWP basis functions on the diabatic states. As in the choice of trajectories (see below), there is some flexibility here; for example, if Ehrenfest trajectories are employed in modeling a system with two electronic states,

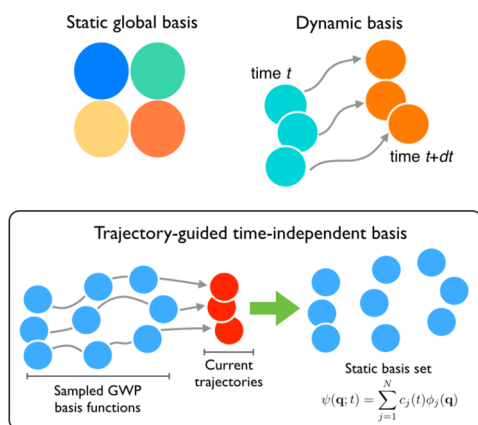


**Figure 1.** Overview of basis set strategies for solving the TDSE; in all cases, the wave function is represented as a linear combination of GWPs, the phase-space positions of which are represented by circles here. In the current work (lower panel), GWPs are positioned during computationally inexpensive trajectory-based simulations in order to generate a nonuniform GWP basis set. The sampled GWPs are then used as a time-independent basis set for solution of the TDSE.

one approach might be to place GWPs on diabatic states  $|1\rangle$  and  $|2\rangle$  with probabilities of  $|a_{12}|^2$  and  $|a_{21}|^2$ , respectively, where  $a_{1,2}$  are the Ehrenfest expansion coefficients for each state. In this work, we chose to place a GWP on each available diabatic state at the same point in the nuclear phase space (on average every  $1/n_s$  time-steps); in other words, when storing GWPs, we simultaneously add  $|\mathbf{g}(\mathbf{q}_i, \mathbf{p}_i; t)\rangle|1\rangle$  and  $|\mathbf{g}(\mathbf{q}_i, \mathbf{p}_i; t)\rangle|2\rangle$  to the full basis set. Our initial calculations have found that this “mirrored” trajectory sampling approach gives a slightly better description of nonadiabatic dynamics than a probabilistic method, probably due to the improved overlap between basis functions on different electronic states. Finally, we note that this idea of “mirrored” trajectories has been employed previously in *ab initio* multiple spawning (AIMS) simulations,<sup>36</sup> although only in the context of improving the description of nonadiabatic population transfer at short times.

### 3. APPLICATION: RESULTS AND DISCUSSION

To demonstrate our approach, we consider nonadiabatic dynamics in two different model systems: the vibronic Hamiltonian description of pyrazine photodynamics, and the spin Boson model. Because of the availability of numerically exact simulations results,<sup>37,38</sup> both models have been previously employed as benchmark problems in the development of new simulations methods. Furthermore, these models are multi-dimensional in nature and require a description of dynamics on coupled electron states; as a result, they provide a stern test of any quantum simulation method. Finally, we note that our approach is trivially exact for one-dimensional problems, for which sampling trajectories with sufficiently high energy can always be used to sample the relevant phase space of the problem.

**3.1. Vibronic Hamiltonian for Pyrazine.** Following excitation from the ground-state  $S_0$  to the second excited electronic state  $S_2$  of pyrazine, the system undergoes a transfer of population from  $S_2$  to the vibronically coupled  $S_1$  state,<sup>39,40</sup> the experimentally observed fast relaxation from  $S_2$  to  $S_1$  is attributed to the presence of a conical intersection and results in a broad  $S_2$  absorption spectrum with little discrete structure evident. To accurately describe the relaxation from  $S_2$  to  $S_1$ , a

vibronic Hamiltonian has been developed that explicitly accounts for all  $f = 24$  nuclear degrees of freedom in the problem, as well as the two electronic excited states; it is this vibronic Hamiltonian that we will consider here.<sup>37</sup>

In the basis of diabatic electronic states, the vibronic Hamiltonian for pyrazine can be written as<sup>37</sup>

$$\hat{H} = \sum_{i=1}^f \left[ -\frac{\omega_i}{2} \frac{\partial^2}{\partial q_i^2} + \frac{\omega_i}{2} q_i^2 \right] + \begin{pmatrix} -\Delta & 0 \\ 0 & \Delta \end{pmatrix} + \sum_{i \in G_1} \begin{pmatrix} a_i & 0 \\ 0 & b_i \end{pmatrix} q_i + \sum_{(i,j) \in G_2} \begin{pmatrix} a_{ij} & 0 \\ 0 & b_{ij} \end{pmatrix} q_i q_j + \sum_{i \in G_3} \begin{pmatrix} 0 & c_i \\ c_i & 0 \end{pmatrix} q_i + \sum_{(i,j) \in G_4} \begin{pmatrix} 0 & c_{ij} \\ c_{ij} & 0 \end{pmatrix} q_i q_j$$

where  $q_i$  is the dimensionless normal-mode coordinate of the  $i$ th vibrational mode,  $\omega_i$  is the associated vibrational frequency, and  $2\Delta$  is the energy separation of the  $S_1$  and  $S_2$  states at the origin of the nuclear coordinate-space. The sets  $a_i$ ,  $b_i$ ,  $c_i$ , and  $a_{ij}$ ,  $b_{ij}$ , and  $c_{ij}$  represent a set of parameters that describe linear and bilinear expansion terms, as well as the related coupling between the states. The  $f$  vibrational modes of the problem are subdivided into groups:  $G_1$  is the set of modes having  $A_g$  symmetry,  $G_2$  is the set of pairs of modes with identical symmetry,  $G_3$  is comprised of a single mode of  $B_{1g}$  symmetry, and  $G_4$  is the set of all pairs of modes for which the product has  $B_{1g}$  symmetry. These subdivisions reflect the fact that a vibrational mode that couples the  $S_1$  state ( $B_{3u}$ ) and the  $S_2$  state ( $B_{2u}$ ) must be of  $B_{1g}$  symmetry. The parameters of the vibronic Hamiltonian description of pyrazine have been determined previously from a combination of experimental data and *ab initio* simulation results.<sup>37</sup>

As a test of our simulation approach, the full-dimensional  $f = 24$ -mode problem presents a formidable challenge; instead, we first consider the simpler model with  $f = 4$  vibrational modes, as has also been considered by several other groups.<sup>16,23,25,29,37,41</sup> In this reduced-dimensional model, the vibronic coupling mode  $\nu_{10a}$  and the three  $A_g$  modes with strongest linear coupling parameters (namely,  $\nu_{6a}$ ,  $\nu_1$ , and  $\nu_{9a}$ ) are included in the model. The initial wave function corresponds to a ground-state vibrational wavepacket projected onto the  $S_2$  state,

$$\psi(\mathbf{q}; t = 0) = \left[ \prod_{k=1}^f \left( \frac{1}{\pi} \right)^{1/4} \exp \left( -\left( \frac{1}{2} \right) q_k^2 \right) \right] |2\rangle \quad (5)$$

Following previous work, we focus on simulating three properties of interest. First, we calculate the autocorrelation function (or survival amplitude),  $C(t)$ , which is defined as

$$C(t) = \langle \psi(0) | \exp \left( -\frac{i\hat{H}t}{\hbar} \right) | \psi(0) \rangle = \langle \psi(0) | \psi(t) \rangle \quad (6)$$

Second, we calculate the  $S_2$  photoabsorption spectrum,  $I(\omega)$ , which is related to the Fourier transform of  $C(t)$ , according to

$$I(\omega) \propto \omega \int_{-\infty}^{+\infty} dt C(t) \exp(-i\omega t) \quad (7)$$

The  $S_2$  photoabsorption spectrum of pyrazine has been measured experimentally;<sup>39,40</sup> however, it has been found that a phenomenological damping factor must be introduced into calculated results in order to reproduce the inherent broadening of the experimental spectrum.<sup>37</sup> Here,  $C(t)$  is multiplied by an exponential function,



$$g(t) = \exp\left(-\frac{|t|}{\tau}\right) \quad (8)$$

where  $\tau$  is a model-dependent damping time constant. We note that the use of the exponential damping factor in the calculation of the absorption spectrum is not an essential feature of our methodology and is included simply for comparison to previous simulations; in fact, the exact and simulated spectra determined with  $g(t) = 1$  show a comparable level of agreement with the results presented here. Furthermore, to remove numerical artifacts in the Fourier transformation of  $C(t)$ , which may arise as a result of the finite simulation time for  $C(t)$ , we also multiply by a cosine sampling function, which is given by

$$h(t) = \cos\left(\frac{\pi t}{2t_{\max}}\right) \quad (9)$$

where  $t_{\max}$  is the maximum simulation time for  $C(t)$ .

The final observable of interest is the diabatic population of the  $S_1$  state. Given the definition of our time-dependent wave function (eq 3), the population of the  $S_1$  state is

$$P_1(t) = \sum_{i,j} c_i^* c_j \langle g_i | g_j \rangle \delta_{\lambda_i,1} \delta_{\lambda_j,1} \quad (10)$$

where  $\lambda_j$  is a label indicating whether the  $j$ th GWP basis function sits on the  $S_1$  state ( $\lambda_j = 1$ ) or  $S_2$  state ( $\lambda_j = 2$ ); clearly, this definition exploits the fact that the diabatic electronic states are orthonormal. The state population  $P_1(t)$  indicates the extent to which the wavepacket, initially on  $S_2$ , has transferred onto the  $S_1$  state; as shown below, it is a sensitive indicator of whether our simulation approach is capable of treating nonadiabatic transitions correctly.

It remains to define the trajectory sampling method that was employed in the simulations of the pyrazine vibronic Hamiltonian remains to be done. Given our interest in modeling systems with multiple electronic states, we restrict ourselves to mean-field (Ehrenfest) trajectories in order to account for nonadiabatic transitions in the sampling trajectories. A similar trajectory approach has been taken in the multiconfiguration Ehrenfest (MCE) method;<sup>16</sup> however, in that case, Ehrenfest trajectories are used to guide a basis set of *time-dependent* GWPs, rather than create a *time-independent* basis set, as in this work.

Here, the initial position and momenta of each of the  $m$  sampling trajectories were sampled from the Wigner distribution of the initial wave function. Restricting our discussion to a system of two electronic diabatic states, each sampling trajectory represents a time-evolving wavepacket constructed as

$$|\phi(t)\rangle = [a_1(t)|1\rangle + a_2(t)|2\rangle] |g(\mathbf{q}_t, \mathbf{p}_t; t)\rangle \quad (11)$$

where  $a_{1,2}$  are expansion coefficients for the  $|1\rangle$  and  $|2\rangle$  diabatic states, respectively. The positions and momenta that define the GWP,  $\mathbf{q}_t$  and  $\mathbf{p}_t$ , evolve according to the mean-field equations of motion,

$$\frac{\partial q_k}{\partial t} = \frac{p_k}{m_k} \quad (12)$$

$$\frac{\partial p_k}{\partial t} = -\frac{\partial V_{\text{Ehr}}}{\partial q_k} \quad (13)$$

where  $V_{\text{Ehr}}$  is a state-averaged potential energy surface that is given by

$$V_{\text{Ehr}} = \frac{|a_1|^2 V_{11} + |a_2|^2 V_{22} + 2\text{Re}(a_1^* a_2 V_{12})}{|a_1|^2 + |a_2|^2} \quad (14)$$

and  $V_{ij}$  is the  $ij$ th matrix element of the potential energy of the system. The expansion coefficients of each state ( $a_{1,2}$ ) evolve according to the TDSE, accounting for the time dependence of the GWP position and momenta:

$$\dot{\mathbf{a}} = -\frac{i}{\hbar} [\mathbf{H} - i\hbar \dot{\mathbf{S}}] \mathbf{a} \quad (15)$$

Here,  $\mathbf{H}$  is the Hamiltonian matrix (in the electronic basis) with elements  $H_{ij} = \langle g_i | i\hbar \hat{H} | g_j \rangle$  and  $\dot{\mathbf{S}}$  is a time-derivative matrix with elements

$$\dot{S}_{ij} = \delta_{ij} \left[ \sum_{\kappa=1}^f \left\langle g_i \left| \frac{\partial g_t}{\partial q_{\kappa}} \right\rangle \frac{\partial q_{\kappa}}{\partial t} + \left\langle g_i \left| \frac{\partial g_t}{\partial p_{\kappa}} \right\rangle \frac{\partial p_{\kappa}}{\partial t} \right] \quad (16)$$

In the simulations presented here, the positions and momenta of the GWP, and the expansion coefficients  $a_{1,2}$ , were evolved using an evolution scheme previously implemented for *ab initio* multiple spawning (AIMS<sup>10–13,36,42–44</sup>) simulations.

All calculations were performed with a time-step of 0.1 fs; sampling trajectories were run for a total of 150 fs and the TDSE was also solved for 150 fs. During each sampling trajectory, the current GWP  $|g(\mathbf{q}_t, \mathbf{p}_t; t)\rangle$  at a given time step was stored with a probability of  $1/n_s$ ; here, we chose  $n_s = 100$  and we note that the final result is reasonably insensitive to the exact value of  $n_s$ . Simulations were repeated using  $m = 100, 400$ , and 750 sampling trajectories, resulting in total sampled basis-set sizes of  $\sim 3000, 12\,000$ , and  $24\,000$  GWPs. For each system size, we performed five independent simulations; the results presented below represent averages over these five runs. In the TDSE simulations, the fourth-order Runge–Kutta integration algorithm was employed to evolve the time-dependent expansion coefficients, and initial expansion coefficients were determined by projection onto the initial wavepacket. Finally, all Hamiltonian matrix elements were calculated analytically, and the fixed widths of all degrees of freedom was  $\gamma = 0.5$ .

Figure 2 illustrates results for the autocorrelation function  $C(t)$  and  $S_2$  photoabsorption spectrum  $I(\omega)$  using our trajectory-based approach. Even for the smallest of these basis sets, we find excellent agreement with the exact (grid-based<sup>29</sup>)  $C(t)$ . As the basis set size is increased, the calculated  $C(t)$  converges toward the exact result, such that, for the largest basis

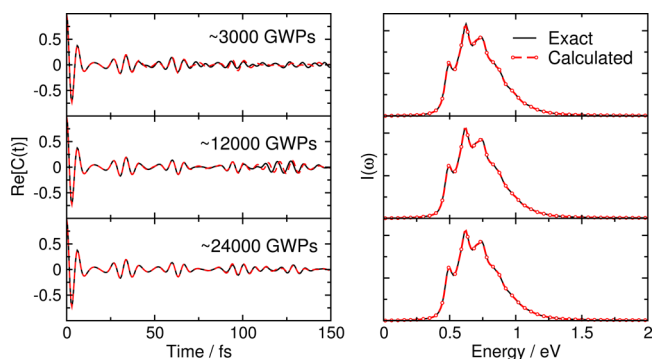


**Figure 2.** Calculated autocorrelation function  $C(t)$  and  $S_2$  photoabsorption spectrum  $I(\omega)$  for four-mode pyrazine vibronic Hamiltonian calculated with  $\sim 3000$  GWPs (top row),  $12\,000$  GWPs (middle row), and  $24\,000$  GWPs (bottom row) sampled for solution of the TDSE.

set employed, the exact and simulated results are almost indistinguishable. Notably, our simulated results are always least accurate at longer times; this is most likely a result of the inherent “spreading-out” of the initial wave function throughout phase-space at longer times, suggesting that the long-time accuracy required will have an important bearing on the necessary number of GWPs in the basis set. However, the long-time inaccuracies observed here may also arise due to the fact that we employ approximate sampling trajectories based on mean-field potential energy surfaces; as is well-known, such quantum/classical trajectories are not guaranteed to possess the correct long-time behavior, principally as a result of errors in treating zero-point energy (ZPE).<sup>45,46</sup> Finally, Figure 2 also shows the results for the  $S_2$  photoabsorption spectrum,  $I(\omega)$ . Most strikingly, we find that even our smallest simulation gives a result that is almost indistinguishable from the exact result; this is clearly a result of the fact that  $I(\omega)$  is calculated using a damped autocorrelation function and, as a result, is less sensitive to errors after a long time in  $C(t)$ . These results further serve to suggest that relying on comparison to exact or experimental spectra for this problem is not a particularly sensitive test of accuracy in a given simulation method.

Figure 3 illustrates the diabatic population of the  $S_1$  state calculated with increasing basis set size. Again, even for the

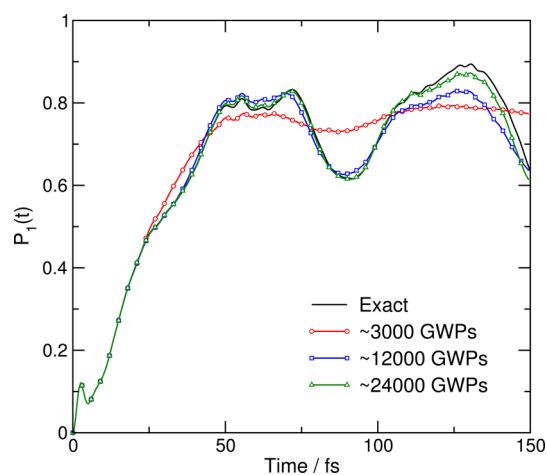


**Figure 3.** Time-dependent population,  $P_1(t)$ , of the lower diabatic state as calculated with three different basis set sizes for the four-mode vibronic pyrazine Hamiltonian.

(very small) total basis set of 3000 GWPs, we observe qualitatively accurate population dynamics; for example, the recurrence at  $\sim 80$  fs is clearly observed, but we find that the long-time populations are somewhat inaccurate. As expected, the quality of the calculation increases as the basis set size increases; 12 000 sampled GWPs give excellent agreement with the overall dynamics, while 24 000 GWPs further improves on this. We note here that the convergence of the population dynamics seems to be much slower than the convergence of  $C(t)$  in Figure 2; this may be a consequence of the fact that  $P_1(t)$  reports on dynamics across the entire intersection of the two diabatic states, whereas  $C(t)$  naturally reports on the wave function behavior in the vicinity of the initial wave function. In any case, the results of Figure 3 clearly demonstrate that our simulation approach is at least qualitatively correct, even for small basis sets, and can be systematically improved upon by simply running more sampling trajectories.

Finally, we consider the full-dimensional ( $f = 24$ ) vibronic Hamiltonian for pyrazine. As noted above, this is an extremely challenging test for any quantum simulation method, requiring accurate description of nuclear and electronic dynamics within a multidimensional space; however, this system serves as an important benchmark due to the availability of numerically exact simulation results from the multiconfigurational time-dependent Hartree (MCTDH) method.<sup>37</sup> Figure 4 illustrates

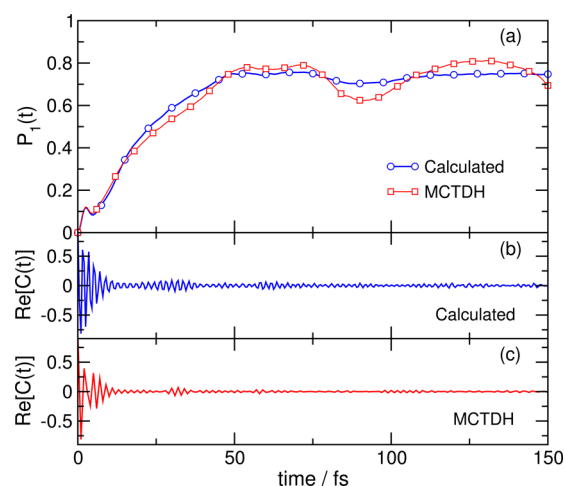


**Figure 4.** (a) Time-dependent population of  $S_1$  state following photoexcitation to the  $S_2$  state in the 24-mode pyrazine vibronic Hamiltonian; results are compared to MCTDH calculations.<sup>37</sup>

the calculated population transfer dynamics and autocorrelation function for our simulations employing 21 000 GWPs generated in 700 Ehrenfest sampling trajectories. As expected, the agreement with MCTDH for this basis set is not perfect, although it is clear that our simple trajectory-guided approach correctly captures the qualitative population dynamics in this multidimensional system, including the population recurrence at  $\sim 80$  fs. The calculated correlation function  $C(t)$  is also in good agreement with the MCTDH results, although the oscillatory structure in our  $C(t)$  calculations appears to be overestimated, compared to MCTDH. Despite this, it is clear that our simple quantum dynamics approach reproduces the behavior of the population dynamics in this 24-dimensional system to a sufficient level of accuracy to infer, for example, the existence of rapid population transfer from  $S_2$  to  $S_1$  via a conical intersection.

Overall, we can conclude, from these simulations, that our trajectory-guided approach can quickly provide qualitatively accurate results using quite small basis sets and can be systematically improved simply by increasing the number of sampling trajectories. Furthermore, we note that we have done little to optimize our approach; alternative choices of trajectory sampling and GWP placement strategies may improve these simulations further. Finally, we note that all calculations performed here have employed full matrix storage; upon going to larger basis set sizes, we can clearly exploit sparsity in the overlap and Hamiltonian matrices required for solution of the TDSE, thereby reducing computational expense.

**3.2. Spin Boson Model.** In the second demonstration of our approach, we choose another challenging problem, namely, the spin Boson (SB) model.<sup>38</sup> The SB Hamiltonian describes a two-level electronic system linearly coupled to a bath of harmonic oscillators; this is the prototypical model of energy

transfer following photoexcitation in a dissipative environment. The SB model represents a tough challenge for our methodology; for example, this many-dimensional system lies beyond the reach of the standard global basis approach of quantum dynamics unless one specifically exploits the form of the potential. The need to perform thermal ensemble-averaging introduces a further test of our trajectory-based method, which must be able to sample appropriate basis functions for a range of different initial thermal wavepackets.

The explicit Hamiltonian for the  $f$ -dimensional SB system is

$$\hat{H} = \epsilon \hat{\sigma}_z + \Delta \hat{\sigma}_x + \hat{\sigma}_z \sum_{k=1}^f c_k q_k + \sum_{k=1}^f \left[ \frac{p_k^2}{2m_k} + \frac{1}{2} m_k \omega_k^2 q_k^2 \right] \quad (17)$$

where  $\hat{\sigma}_x$  and  $\hat{\sigma}_z$  are the usual Pauli spin matrices,  $\omega_k$  is the frequency of the  $k$ th oscillator, and  $c_k$  is the corresponding coupling parameter between the oscillator and the electronic subsystem. The harmonic bath is characterized through its spectral density,  $J(\omega)$ ; in the present work, we use a Debye spectral density of the form

$$J(\omega) = \frac{\eta \omega_c \omega}{(\omega^2 + \omega_c^2)} \quad (18)$$

where  $\eta$  is the coupling strength between the bath and the electronic subsystem, and  $\omega_c$  is the cutoff frequency. The bath is discretized into  $f = 30$  modes with the bath frequencies ( $\omega_k$ ) given by

$$\omega_k = \omega_c \tan \left[ \frac{\pi}{2f} \left( k - \frac{1}{2} \right) \right] \quad (19)$$

and the coupling strengths ( $c_k$ ) given by

$$c_k = \omega_k \sqrt{\frac{\eta}{f}} \quad (20)$$

This discretization scheme ensures that the exact electronic reorganization energy is obtained.<sup>18,47–49</sup> Finally, all degrees of freedom have mass  $m_k = 1$ , we employ atomic units such that  $\hbar = k_B = 1$ , and units are given relative to the interstate coupling value  $\Delta$ .

The time-dependent property of interest is the thermally averaged population difference between the two excited states, given by

$$P(t) = \frac{1}{Z_B} \text{Tr} \left[ \exp(-\beta \hat{H}_b) |1\rangle \langle 1| \exp \left( + \frac{i\hat{H}t}{\hbar} \right) \hat{\sigma}_z \exp \left( - \frac{i\hat{H}t}{\hbar} \right) \right] \quad (21)$$

Here, the initial Boltzmann density operator is chosen such that the system is prepared in an equilibrium state for the bath degrees of freedom (so  $\hat{H}_b$  corresponds to the final summation of eq 17) and the system then undergoes a Franck–Condon transition to the excited state  $|1\rangle$ . Inserting complete sets of coordinate eigenstates allows one to write  $P(t)$  as

$$P(t) = \frac{1}{Z_B} \int d\mathbf{q} d\mathbf{q}_1 [P_1(\mathbf{q}; t) - P_2(\mathbf{q}; t)] \quad (22)$$

where

$$P_k(\mathbf{q}; t) = \frac{\left| \langle k | \mathbf{q} | \exp \left[ \left( - \frac{\beta \hat{H}_b}{2} \right) - \left( \frac{i\hat{H}t}{\hbar} \right) \right] | \mathbf{q}_1 \rangle \right|^2}{Z_B} \quad (23)$$

As shown in recent work,<sup>18</sup> the initial population function  $P_1(t = 0)$  may be generated quite straightforwardly in a path-integral molecular dynamics (PIMD) simulation. In particular,  $P_1(t = 0)$  is proportional to the density of points at imaginary-time values of  $\beta/2$ , following propagation from a fixed point  $\mathbf{q}_1$ ; by assuming a Gaussian density distribution, as is common in approaches such as the variational Gaussian method of Mandelshtam and co-workers,<sup>50–53</sup>  $P_1(t = 0)$  may be easily calculated in a constrained equilibrium path-integral calculation. Because the real-time evolution of  $P_1(t = 0)$  obeys the TDSE, the trajectory-based simulation method proposed here may be used to propagate this initial thermal wavepacket; eq 22 indicates that averaging  $P(t)$  over many such initial wavepackets allows one to calculate the thermally averaged time-dependent population difference.

In the calculations illustrated here, we considered three different sets of SB model parameters for which numerically exact simulation results are available.<sup>38</sup> In set (a), corresponding to the intermediate ( $\omega_c/\Delta \approx 1$ ) bath regime, we chose  $\omega_c = 1.0$ ,  $\eta = 5.0$ ,  $\beta = 1.0$ , and  $\epsilon = 0.0$ . In set (b), we chose  $\omega_c = 0.25$ ,  $\eta = 5.0$ ,  $\beta = 5.0$ , and  $\epsilon = 0.0$ , corresponding to the adiabatic bath regime ( $\omega_c/\Delta < 1$ ). Finally, in set (c), we chose  $\omega_c = 5.0$ ,  $\eta = 0.5$ ,  $\beta = 0.5$ , and  $\epsilon = 1.0$ , giving an example of a SB model with a nonzero bias between the energies of the diabatic electronic states. For these simulations, the initial thermal wavepacket was generated in a constrained PIMD simulation using 250 ring-polymer beads (or Trotter slices), 8–12 GWP sampling trajectories were initiated for each thermal GWP, and propagation results for 1000 initial thermal GWPs were averaged to give the final thermal population functions. In all calculations, the widths of the sampled GWPs were set to be identical to the widths of the initial thermal wavepacket, as sampled by path-integral sampling.<sup>18</sup>

To demonstrate that our approach is flexible, with regard to the sampling trajectories employed, we used simple classical trajectories initiated on the  $|1\rangle$  and  $|2\rangle$  diabatic states alternately in order to generate a GWP basis set for propagation of each initial thermal wavepacket. In total, our calculations employed a basis set of 1800–2400 GWPs for each initial thermal wavepacket. Following our previous work,<sup>18</sup> we note that, because our sampling strategy for generating initial thermal wavepackets only yields the *density*, the choice of initial momenta for the GWP sampling trajectories is somewhat arbitrary. In this work, we chose to sample from the classical Boltzmann distribution in the case of (b) and (c), and from the Wigner distribution in the case of (a). Finally, for comparison, we calculated the time-dependent populations using the Ehrenfest (mean-field) approach with initial bath conditions sampled from the Wigner distribution and final populations averaged over 2000 trajectories.<sup>54</sup>

Figure 5 shows the results of our trajectory-guided simulations for the SB model. As expected, based on our experiences with the pyrazine model, we find that our simple simulation strategy, combined with path-integral sampling of initial thermal GWPs, can capture the qualitatively correct quantum dynamics in each case. The agreement with the exact results in the intermediate regime (Figure 5a) is surprisingly good, and clearly better than the standard Ehrenfest approach.



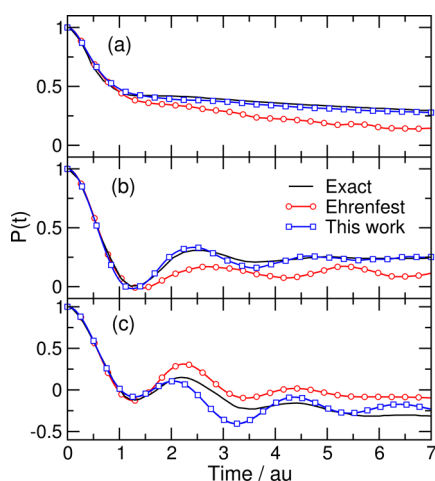


**Figure 5.** Population difference functions  $P(t)$  calculated in trajectory-guided quantum simulations of the SB model with parameters chosen to give (a) the intermediate bath regime, (b) the adiabatic bath regime, and (c) a nonzero energetic bias between the electronic states. In each panel, results are shown for numerically exact simulations,<sup>38</sup> the Ehrenfest method, and our trajectory-guided approach.

Similarly, in the adiabatic bath regime (Figure 5b), our simulations clearly capture the oscillations in the diabatic state populations and the long-time limit is in much better agreement with the exact result than the Ehrenfest result is. Finally, we find that our simple approach can reproduce the qualitative population dynamics in the asymmetric SB model (Figure 5c); the agreement with the exact result here is much better than the Ehrenfest result, but is clearly not as good as in the two other cases considered. The most likely explanation for this is our dependence on classical trajectories to place basis functions. It is well-known that methods based on classical trajectories can fail to correctly describe long-time dynamics in nonzero-bias SB models as a result of errors in the treatment of ZPE;<sup>45,46,54</sup> as a result, it seems likely that the long-time accuracy of our trajectory-based approach may suffer, because basis functions are increasingly placed in regions of phase space that are not consistent with the exact quantum dynamics of the system. However, we note that, unlike the Ehrenfest method and similar approaches where classical trajectories are used to directly construct quantum information, our approach can be made increasingly accurate by simply increasing the number of sampled GWPs. A more efficient alternative is clearly to choose trajectory-generation methods that result in more accurate sampling of the relevant phase space at longer times; one example might be RPMD,<sup>55,56</sup> which yields the exact quantum Boltzmann distribution,<sup>57</sup> although this is clearly an avenue for further work.

Overall, we find that the performance of our trajectory-guided simulation approach is better than the established Ehrenfest method, and it performs comparably to other methods that are specifically adapted to work for system-bath models.<sup>54</sup> This level of performance is particularly encouraging, given that we have done little to optimize our approach.

**Computational Effort.** As a final point, it is worth considering how our approach fares, in terms of computational expense. Running  $m$  trajectories of length  $n_t$  time steps, followed by solution of the TDSE for  $n_t$  time steps, will require a total computational time  $t$  of approximately

$$t = amn_t + b\left(\frac{mn_t}{n_s}\right)^3 + cn_t\left(\frac{mn_t}{n_s}\right)^2 \quad (24)$$

where  $a$ ,  $b$ , and  $c$  are characteristic constants representing the time for performing one time step of a trajectory, calculating Hamiltonian, overlap and inverse overlap matrices, and propagation of the complex expansion coefficients by continued matrix-vector multiplication, respectively. (Note that we have assumed the worst-case scenario for matrix manipulations.) Note that the overall effort of the approach does not explicitly depend on the number of degrees of freedom in the system; the system dependence is instead reflected in the number of GWPs, which will be required to obtain converged results. In many applications, generating classical (or related) trajectories is relatively inexpensive from the computational viewpoint; instead, the computational expense of our approach is dominated by construction of the Hamiltonian, overlap and inverse overlap matrices, as well as propagation by large-scale matrix-vector multiplications. However, there is much scope to improve all of these bottlenecks; for example, the Hamiltonian and overlap matrices will generally be sparse, particularly in higher-dimensional problems, allowing efficient sparse matrix methodologies to be employed. Furthermore, there is scope to employ potential energy information generated during the course of sampling trajectories in the evaluation of Hamiltonian matrix elements, as in the “Grow” method.<sup>58</sup> Each of these features will make large savings in the computational time of our simulations and are currently being explored.

#### 4. CONCLUSIONS

In this article, we have demonstrated a very simple approach to modeling (nonadiabatic) quantum dynamics in many-dimensional systems using trajectory-guided basis sets. Our results show that, using simple Ehrenfest or classical MD trajectories, the basis sets produced are compact and suitable for solution of the TDSE. An important advantage (or, perhaps, disadvantage) of this approach is its flexibility; we are free to generate the basis set using any trajectory-based method we see fit, and the size of the basis set is also under our control. In the future, we will investigate the use of surface hopping<sup>59</sup> and AIMS<sup>10–13,36,42–44</sup> trajectories as the next level of approximation, although we could also consider using variational GWP trajectories. Finally, we note that both problems considered here are somewhat simplified by having a known set of diabatic states available; current work is aimed at combining our trajectory-based approach with *ab initio* electronic structure calculations for the potential energy surfaces and their couplings. Taking into account the efficiency of our trajectory-based method, this overall methodology should prove useful in modeling quantum chemical dynamics in a variety of systems, particularly photochemical reactions in solvent environments, where there is often a clear distinction between the quantum system and an environment, which can be treated classically.

While straightforward application of our approach has been shown to reproduce qualitative quantum dynamics in many-dimensional problems, there are some clear avenues that could be explored to improve our methodology. First, there is nothing in our current approach to prevent regions of phase space being either undersampled or oversampled by basis functions. While sparse sampling can, in principle, be addressed by increasing the number of sampling trajectories, this may be inefficient. Instead,

we are currently exploring methods whereby further GWP basis functions can be generated to “fill in” sparsely sampled regions of phase space without performing further trajectory simulations; one obvious approach is to exploit the fact that sampled GWPs can be used in a configuration interaction-type framework, whereby orbitals from two different sampled GWPs are swapped to generate new intermediate GWPs. These methods will increase the total size of the basis set but, as noted above, will also benefit from employing sparse matrix methods. In contrast, oversampling in regions of phase space may lead to linear dependence in the basis set; at the moment, we are currently seeking to address this challenge by implementing a recently proposed projection method for dealing with linear dependence in GWP basis sets.<sup>17</sup> Second, it is clear that the time scale over which classical-like trajectories can be used to effectively sample the relevant regions of phase space for wave function propagation will be somewhat problem-dependent; for example, in systems possessing strongly coupled vibrational degrees of freedom, nonphysical flow of ZPE<sup>57</sup> in classical trajectories might mean that sampling basis functions at longer times becomes more difficult. We are currently exploring the possibility of using shorter time segments for trajectory sampling, between which new sampling trajectories are initiated from the current wave function; while this methodology is more akin to the BEL approach,<sup>27</sup> an important difference is that our basis-set sampling approach is based on computationally inexpensive yet physically appropriate trajectories. Overall, these developments have the potential to make an important to the performance of our approach, both in terms of computational expense and accuracy.

## AUTHOR INFORMATION

### Corresponding Author

\*E-mail: S.Habershon@warwick.ac.uk.

### Notes

The authors declare no competing financial interest.

## ACKNOWLEDGMENTS

This research was supported by start-up funding from the University of Warwick (S.H.), and the award of an EPSRC studentship (M.A.C.S.). Computational resources were provided by the Centre for Scientific Computing at the University of Warwick.

## REFERENCES

- (1) Tannor, D. J. *Introduction to Quantum Mechanics: A Time-Dependent Perspective*; University Science Books: Sausalito, CA, 2007.
- (2) Park, T. J.; Light, J. C. *J. Chem. Phys.* **1986**, *85*, 5870.
- (3) Sielk, J.; von Horsten, H. F.; Kruger, F.; Schneider, R.; Hartke, B. *Phys. Chem. Chem. Phys.* **2009**, *3*, 463–475.
- (4) Schmidt, P. P. *Int. J. Quantum Chem.* **2002**, *90*, 202.
- (5) Meyer, H.-D.; Gatti, F.; Worth, G. A., Eds. *Multidimensional Quantum Dynamics: MCTDH Theory and Applications*; Wiley: Weinheim, Germany, 2009.
- (6) Meyer, H.-D.; Manthe, U.; Cederbaum, L. *Chem. Phys. Lett.* **1990**, *165*, 73–78.
- (7) Gerber, R. B.; Buch, V.; Ratner, M. A. *J. Chem. Phys.* **1982**, *77*, 3022.
- (8) Heller, E. J. *J. Chem. Phys.* **1981**, *75*, 2923.
- (9) Jungwirth, P.; Gerber, R. *J. Chem. Phys.* **1995**, *102*, 6046.
- (10) Martinez, T. J.; Ben-Nun, M.; Levine, R. D. *J. Phys. Chem.* **1996**, *100*, 7884.
- (11) Martinez, T. J.; Ben-Nun, M.; Ashkenazi, G. *J. Chem. Phys.* **1996**, *104*, 2847.
- (12) Martinez, T. J. *Chem. Phys. Lett.* **1997**, *272*, 139.
- (13) Martinez, T. J.; Levine, R. D. *J. Chem. Soc., Faraday Trans.* **1997**, *93*, 941.
- (14) Ben-Nun, M.; Martinez, T. J. *Adv. Chem. Phys.* **2002**, *121*, 439.
- (15) Sherratt, P. A.; Shalashilin, D. V.; Child, M. S. *Chem. Phys.* **2006**, *322*, 127.
- (16) Shalashilin, D. V. *J. Chem. Phys.* **2010**, *132*, 244111.
- (17) Habershon, S. *J. Chem. Phys.* **2012**, *136*, 014109.
- (18) Habershon, S. *J. Chem. Phys.* **2013**, *139*, 104107.
- (19) Broeckhove, J.; Lathouwers, L.; Kesteloot, E.; Van Leuven, P. *Chem. Phys. Lett.* **1988**, *149*, 547–550.
- (20) Dirac, P. A. M. *Proc. Cambridge Philos. Soc.* **1930**, *26*, 376.
- (21) Frenkel, J. *Wave Mechanics*; Oxford University Press: Oxford, U.K., 1934.
- (22) McLachlan, A. D. *Mol. Phys.* **1964**, *8*, 39.
- (23) Burghardt, I.; Giri, K.; Worth, G. A. *J. Chem. Phys.* **2008**, *129*, 174104.
- (24) Worth, G. A.; Burghardt, I. *Chem. Phys. Lett.* **2003**, *368*, 502.
- (25) Worth, G. A.; Robb, M. A.; Lasorne, B. *Mol. Phys.* **2008**, *106*, 2077.
- (26) Mendive-Tapia, D.; Lasorne, B.; Worth, G. A.; Robb, M. A.; Bearpark, M. J. *J. Chem. Phys.* **2012**, *137*, 22A548.
- (27) Koch, W.; Frankcombe, T. J. *Phys. Rev. Lett.* **2013**, *110*, 263202.
- (28) Wu, Y.; Batista, V. S. *J. Chem. Phys.* **2003**, *118*, 6720–6724.
- (29) Chen, X.; Batista, V. S. *J. Chem. Phys.* **2006**, *125*, 124313.
- (30) Herman, M. F.; Kluk, E. *Chem. Phys.* **1984**, *91*, 27–34.
- (31) Kay, K. G. *J. Chem. Phys.* **1994**, *100*, 4377.
- (32) Miller, W. H. *J. Phys. Chem. A* **2001**, *105*, 2942–2955.
- (33) Miller, W. H. *J. Phys. Chem. B* **2002**, *106*, 8132.
- (34) Iyengar, S. S.; Sumner, I.; Jakowski, J. *J. Phys. Chem. B* **2008**, *112*, 7601–7613.
- (35) Li, X.; Oomens, J.; Eyler, J. R.; Moore, D. T.; Iyengar, S. S. *J. Chem. Phys.* **2010**, *132*, 244301.
- (36) Ben-Nun, M.; Martinez, T. J. *Isr. J. Chem.* **2007**, *47*, 75–88.
- (37) Raab, A.; Worth, G. A.; Meyer, H.-D.; Cederbaum, L. S. *J. Chem. Phys.* **1999**, *110*, 936–946.
- (38) Thoss, M.; Wang, H.; Miller, W. H. *J. Chem. Phys.* **2001**, *115*, 2991–3005.
- (39) Yamazaki, I.; Murao, T.; Yamanaka, T.; Yoshihara, K. *Faraday Discuss. Chem. Soc.* **1983**, *75*, 395–405.
- (40) Innes, K. K.; Ross, I. G.; Moomaw, W. R. *J. Mol. Spectrosc.* **1988**, *132*, 492–544.
- (41) Puzari, P.; Sarkar, B.; Adhikari, S. *J. Chem. Phys.* **2006**, *125*, 194316.
- (42) Ben-Nun, M.; Martinez, T. J. *J. Chem. Phys.* **1998**, *108*, 7244.
- (43) Ben-Nun, M.; Quenneville, J.; Martinez, T. J. *J. Phys. Chem. A* **2000**, *104*, 5161.
- (44) Ben-Nun, M.; Martinez, T. J. *J. Chem. Phys.* **2000**, *112*, 6113.
- (45) Müller, U.; Stock, G. *J. Chem. Phys.* **1999**, *111*, 77–88.
- (46) Golosov, A. A.; Reichman, D. R. *J. Chem. Phys.* **2001**, *114*, 1065–1074.
- (47) Craig, I. R.; Manolopoulos, D. E. *J. Chem. Phys.* **2005**, *122*, 084106.
- (48) Markland, T. E. *Two different approaches to electronically non-adiabatic dynamics*. M.Sc. Thesis, Oxford University, Oxford, U.K., 2006.
- (49) Wang, H.; Thoss, M.; Miller, W. H. *J. Chem. Phys.* **2001**, *115*, 2979–2990.
- (50) Brown, S. E.; Georgescu, I.; Mandelshtam, V. A. *J. Chem. Phys.* **2013**, *138*, 044317.
- (51) Georgescu, I.; Deckman, J.; Fredrickson, L. J.; Mandelshtam, V. A. *J. Chem. Phys.* **2011**, *134*, 174109.
- (52) Frantsuzov, P. A.; Mandelshtam, V. A. *J. Chem. Phys.* **2008**, *128*, 094304.
- (53) Frantsuzov, P. A.; Mandelshtam, V. A. *J. Chem. Phys.* **2004**, *121*, 9247–9256.



- (54) Berkelbach, T. C.; Reichman, D. R.; Markland, T. E. *J. Chem. Phys.* **2012**, *136*, 034113.
- (55) Habershon, S.; Manolopoulos, D. E.; Markland, T. E.; Miller, T. F. *Annu. Rev. Phys. Chem.* **2013**, *64*, 387–413.
- (56) Craig, I. R.; Manolopoulos, D. E. *J. Chem. Phys.* **2004**, *121*, 3368–3373.
- (57) Habershon, S.; Manolopoulos, D. E. *J. Chem. Phys.* **2009**, *131*, 244518.
- (58) Frankcombe, T. J.; Collins, M. A.; Worth, G. A. *Chem. Phys. Lett.* **2010**, *489*, 242–247.
- (59) Tully, J. C. *J. Chem. Phys.* **1990**, *93*, 1061–1071.